Journal of Applied Physics

Magnetization reversal dynamics in the media of magneto-optical recording

Cite as: Journal of Applied Physics **63**, 5809 (1988); https://doi.org/10.1063/1.340320
Submitted: 29 October 1987 . Accepted: 02 February 1988 . Published Online: 04 June 1998

M. Mansuripur

View Online Export Citation

ARTICLES YOU MAY BE INTERESTED IN

The design and verification of MuMax3
AIP Advances **4**, 107133 (2014); https://doi.org/10.1063/1.4899186

Exchange spring media for perpendicular recording
Applied Physics Letters **87**, 012504 (2005); https://doi.org/10.1063/1.1951053

Magnetic and magneto-optical properties of rare-earth transition-metal alloys containing Gd, Tb, Fe, Co
Journal of Applied Physics **66**, 756 (1989); https://doi.org/10.1063/1.343551

Ultra High Performance SDD Detectors

AMETEK MATERIALS ANALYSIS DIVISION

See all our XRF Solutions

© 1988 American Institute of Physics.

AIP Publishing

Magnetization reversal dynamics in the media of magneto-optical recording

M. Mansuripur
Boston University, College of Engineering, 44 Cummington Street, Boston, Massachusetts 02215

(Received 29 October 1987; accepted for publication 2 February 1988)

Domain wall dynamics in thin films of amorphous rare-earth–transition-metal alloys are investigated using numerical integration of the Landau–Lifshitz–Gilbert equation. A two-dimensional square lattice of dipoles with nearest-neighbor exchange interaction and random axis anisotropy is simulated and the structure of domain walls (with and without Bloch lines) is determined. The motion of domain walls under applied fields is then considered and the effects of random spatial variations of magnetic parameters upon wall mobility are discussed.

I. INTRODUCTION

The process of magnetization reversal in thin films of amorphous rare-earth–transition-metal alloys is of considerable importance in the area of erasable optical data storage.[1–5] Thermomagnetic recording consists of laser-induced nucleation and growth of reverse magnetized domains under the influence of external and/or internal magnetic fields.[6–9] The nature of the nucleation process, speed and uniformity of growth, and local pinning of domain boundaries due to structural inhomogeneities of the material are among factors that determine the final shape and size of the recorded domain. Since it is important to control the domain size while avoiding nonuniformities and jagged boundaries, and since it is important to create stable domains, a knowledge of magnetization reversal dynamics including the effects of amorphous structure is highly desirable.

In this paper we present computer simulations of a model based on the Landau–Lifshitz–Gilbert equation of magnetization dynamics. The model incorporates random features of amorphous materials and gives a quantitative description of the reversal process. Our algorithm is particularly suited for programming on a highly parallel computer such as the Connection Machine[10,11]; in fact, for large scale simulations, such special purpose hardware and/or supercomputers are indispensable. However, it is possible to show the feasibility of the concept using ordinary computers. The small scale simulations reported here were obtained on a VAX 11/780 machine.

In the next section we derive the equations needed for the description of the algorithm. Then, in Sec. III we derive analytic results pertaining to the statics and dynamics of domain walls under various approximations. This analysis identifies the range of validity of the approximate solutions and provides results for comparison with the simulations in certain limiting regimes. Section IV gives a description of the algorithm and presents the simulation results.

II. MAGNETIZATION DYNAMICS IN A DISCRETE LATTICE OF INTERACTING DIPOLES

The Landau–Lifshitz–Gilbert (LLG) equation is believed to embody the governing mechanisms of magnetization dynamics.[12] This equation describes the motion of a dipole in the presence of a net equivalent magnetic field. In the following subsections we derive the equivalent field for a square lattice of interacting dipoles which is then used in the LLG equation to yield suitable formulas for the numerical analysis of the dynamic process. We also show that the energy of the system driven by the LLG equation is a nonincreasing function of time.

A. Effective magnetic fields

We derive expressions for the effective magnetic fields acting on individual moments in a two-dimensional square lattice. These arise from the applied field, local anisotropy, nearest-neighbor exchange, and classical dipole-dipole interactions. The sum of these four contributions is the net field with components in the r, θ, and ϕ directions of the spherical coordinate system. Since only the torque induced by the field is of interest in this work, and since the component of the field along the magnetization direction does not contribute to the torque, we shall define the r direction to be that of the magnetization vector at the given lattice site and therefore ignore the r component of the field. Thus, in the following analysis, only the θ and ϕ components of the field are evaluated.

The following relationships hold between the unit vectors of a Cartesian coordinate system and those of a spherical coordinate system:

$$\hat{i}_r = \sin\theta\cos\phi\,\hat{i}_x + \sin\theta\sin\phi\,\hat{i}_y + \cos\theta\,\hat{i}_z, \tag{1a}$$

$$\hat{i}_\theta = \cos\theta\cos\phi\,\hat{i}_x + \cos\theta\sin\phi\,\hat{i}_y - \sin\theta\,\hat{i}_z, \tag{1b}$$

$$\hat{i}_\phi = -\sin\phi\,\hat{i}_x + \cos\phi\,\hat{i}_y. \tag{1c}$$

Assuming an external field $\mathbf{H}_{\rm ext} = H_x\hat{i}_x + H_y\hat{i}_y + H_z\hat{i}_z$ acting at the lattice site (i,j) with magnetization vector $\mathbf{M} = M_0\hat{i}_r$, the θ and ϕ components of the field are

$$H_\theta^{(\rm ext)} = \mathbf{H}_{\rm ext}\cdot\hat{i}_\theta = H_x\cos\theta\cos\phi + H_y\cos\theta\sin\phi - H_z\sin\theta, \tag{2a}$$

$$H_\phi^{(\rm ext)} = \mathbf{H}_{\rm ext}\cdot\hat{i}_\phi = -H_x\sin\phi + H_y\cos\phi. \tag{2b}$$

Next we calculate the contribution of the uniaxial magnetic anisotropy to the effective field at a given site. Let the local axis of anisotropy have an arbitrary direction in space, specified in spherical coordinates as $\hat{i}_{r_0}$ with angular coordinates (θ_0,ϕ_0). The magnetization vector at this site is

 0021-8979/88/125809-15$02.40 © 1988 American Institute of Physics

$\mathbf{M} = M_0 \hat{i}_r$ with angular coordinates (θ,ϕ). Using K_u as the uniaxial anisotropy constant, the anisotropy energy density can be written as[13]

$$W_{\text{ans}} = K_u [1 - (\hat{i}_r \cdot \hat{i}_{r_0})^2]$$
$$= K_u \{1 - [\cos\theta \cos\theta_0 + \sin\theta \sin\theta_0 \times \cos(\phi - \phi_0)]^2\}. \quad (3)$$

In order to obtain an equivalent field $\mathbf{H}$ for anisotropy, let us assume that $\mathbf{M}$ rotates by a small amount $(\Delta\theta,\Delta\phi)$. The change in energy density is then given by:

$$\Delta W = -\mathbf{H}\cdot\Delta\mathbf{M} = -(H_r \hat{i}_r + H_\theta \hat{i}_\theta + H_\phi \hat{i}_\phi) \cdot (|\mathbf{M}|\Delta\theta \hat{i}_\theta + |\mathbf{M}|\sin\theta\Delta\phi \hat{i}_\phi)$$
$$= -|\mathbf{M}|H_\theta \Delta\theta - |\mathbf{M}|H_\phi \sin\theta\Delta\phi.$$

Consequently:

$$\frac{\partial W}{\partial\theta} = -|\mathbf{M}|H_\theta, \quad (4a)$$

$$\frac{\partial W}{\partial\phi} = -|\mathbf{M}|\sin\theta H_\phi. \quad (4b)$$

Equations (4a) and (4b) are quite general and give components of the equivalent field in terms of the corresponding energy density. For anisotropy, these components are

$$H_\theta^{(\text{ans})} = -(K_u/|\mathbf{M}|)\{\sin 2\theta \times [\cos^2\theta_0 - \sin^2\theta_0 \cos^2(\phi - \phi_0)] - \cos 2\theta \sin 2\theta_0 \cos(\phi - \phi_0)\}, \quad (5a)$$

$$H_\phi^{(\text{ans})} = -(K_u/|\mathbf{M}|)[\sin\theta \sin^2\theta_0 \sin 2(\phi - \phi_0) + \cos\theta \sin 2\theta_0 \sin(\phi - \phi_0)]. \quad (5b)$$

Although the field as given by Eq. (5) is complicated, one can check its validity by looking at some special cases. For instance, when $\phi - \phi_0 = n\pi$, we find that $H_\theta^{(\text{ans})} = -(K_u/|\mathbf{M}|)\sin 2[\theta - (-1)^n\theta_0]$ and $H_\phi^{(\text{ans})} = 0$. Clearly the field is in the direction of $\hat{i}_\theta$ and tries to pull the magnetization toward the easy axis through the shortest path.

Calculation of the exchange contribution to the equivalent field must proceed by first expressing the exchange energy density in terms of orientations of the coupled moments. Let $\mathbf{M}$ and $\mathbf{M}_1$ be two neighboring moments on the lattice with distance d between them and let A_x represent the macroscopic exchange stiffness coefficient.[13,14] The exchange energy density for this pair is then written as

$$W_{xhg} = \frac{2A_x}{d^2}\left(1 - \frac{\mathbf{M}}{|\mathbf{M}|}\cdot\frac{\mathbf{M}_1}{|\mathbf{M}_1|}\right), \quad (6a)$$

or, in terms of the spherical coordinates of the corresponding moments,

$$W_{xhg} = (2A_x/d^2)(1 - \hat{i}_r \cdot \hat{i}_{r_1})$$
$$= (2A_x/d^2)[1 - \cos\theta\cos\theta_1 - \sin\theta\sin\theta_1\cos(\phi - \phi_1)]. \quad (6b)$$

This energy density can now be differentiated to yield the effective exchange field on $\mathbf{M}$ as a result of interaction with $\mathbf{M}_1$. Using Eqs. (4) we obtain

$$H_\theta^{(xhg)} = -(2A_x/|\mathbf{M}|d^2)[\sin\theta\cos\theta_1 - \cos\theta\sin\theta_1\cos(\phi - \phi_1)], \quad (7a)$$

$$H_\phi^{(xhg)} = -(2A_x/|\mathbf{M}|d^2)\sin\theta_1\sin(\phi - \phi_1). \quad (7b)$$

Again it is interesting to note that in the special cases the above expressions reduce to intuitively expected forms. For instance when $\theta_1 = 0$ or π we have $H_\theta^{(xhg)} = \pm(2A_x/|\mathbf{M}|d^2)\sin\theta$ and $H_\phi^{(xhg)} = 0$; or when $\phi - \phi_1 = n\pi$, $H_\theta^{(xhg)} = -(2A_x/|\mathbf{M}|d^2)\sin[\theta - (-1)^n\theta_1]$ and $H_\phi^{(xhg)} = 0$. In all these cases the effective field tries to pull the moment $\mathbf{M}$ towards $\mathbf{M}_1$ through the shortest path.

Finally, we calculate the demagnetizing field of a dipole $\mathbf{m}_1$, located in the xy plane of the lattice at $(x_1 = l\cos\psi, y_1 = l\sin\psi)$, on another dipole $\mathbf{m}$ located at the origin $(x = 0, y = 0)$. Let $\mathbf{n}$ be the unit vector along the line connecting the origin to (x_1, y_1) as shown in Fig. 1. Then

$$\mathbf{n} = \cos\psi \hat{i}_x + \sin\psi \hat{i}_y. \quad (8a)$$

The demagnetizing field at the origin is related to $\mathbf{m}_1$ and $\mathbf{n}$ as follows[15]:

$$\mathbf{H}^{(\text{dmag})} = [3\mathbf{n}(\mathbf{n}\cdot\mathbf{m}_1) - \mathbf{m}_1]/l^3. \quad (8b)$$

From Eqs. (1) and (8), we find

$$H_\theta^{(\text{dmag})} = \mathbf{H}^{(\text{dmag})}\cdot\hat{i}_\theta = (|\mathbf{m}_1|/l^3)[3(\mathbf{n}\cdot\hat{i}_{r_1})(\mathbf{n}\cdot\hat{i}_\theta) - (\hat{i}_{r_1}\cdot\hat{i}_\theta)], \quad (9a)$$

$$H_\phi^{(\text{dmag})} = \mathbf{H}^{(\text{dmag})}\cdot\hat{i}_\phi = (|\mathbf{m}_1|/l^3)[3(\mathbf{n}\cdot\hat{i}_{r_1})(\mathbf{n}\cdot\hat{i}_\phi) - (\hat{i}_{r_1}\cdot\hat{i}_\phi)], \quad (9b)$$

or equivalently:

$$H_\theta^{(\text{dmag})} = (hd^2|\mathbf{M}_1|/l^3)\{\sin\theta\cos\theta_1 + \cos\theta\sin\theta_1 \times [3\cos(\phi - \psi)\cos(\phi_1 - \psi) - \cos(\phi - \phi_1)]\}, \quad (10a)$$

$$H_\phi^{(\text{dmag})} = (hd^2|\mathbf{M}_1|/l^3)\sin\theta_1 \times [\sin(\phi - \phi_1) - 3\sin(\phi - \psi)\cos(\phi_1 - \psi)]. \quad (10b)$$

Here hd^2 is the volume of a cell in the lattice which, when multiplied by the magnetization $\mathbf{M}_1$, gives the strength of the dipole moment $\mathbf{m}_1$ at that lattice site. Again, one may check the validity of Eqs. (10a) and (10b) by considering some special cases.

The total demagnetizing field on any given dipole in the lattice is the sum of the demagnetizing field of all the other

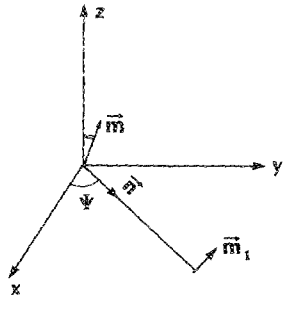

FIG. 1. Assumed positions of two dipoles $\mathbf{m}$ and $\mathbf{m}_1$ in the xy plane of the lattice for calculation of the demagnetizing field. $\mathbf{m}$ is at the origin and its orientation is specified by the spherical coordinates θ and ϕ. $\mathbf{m}_1$ is a distance l away from the origin and its orientation is specified by θ_1 and ϕ_1. The angular coordinate of the line joining the two dipoles is ψ. All three angles ϕ, ϕ_1, and ψ are measured from the positive x axis.

dipoles calculated at the given site. Since the strength of dipole-dipole interaction drops with distance as $1/l^3$ whereas the number of dipoles at a distance l in two dimensions grows only linearly with l, it is not necessary to include the contribution of the entire lattice in the demagnetizing field calculations. Thus, we define significant neighbors (sn) as those neighbors whose contribution to the demagnetizing field is substantial; typically, these include the dipoles within a radius of ten or so lattice constants from the given site.[3] Confining the dipole-dipole interaction to significant neighbors constitutes a major reduction in the required amount of computation, yet it fails to bring large scale simulations within the reach of conventional (sequential) computers. A parallel machine such as the Connection Machine with several thousand processors that can communicate efficiently among themselves, however, is the perfect environment for these simulations. At the time of this writing only a few Connection Machines exist and access to them is extremely limited; moreover, appropriate software tools are still under development. Nevertheless, there is widespread belief that the Connection Machine and similar architectures will soon become the mainstream of parallel computing. It is only in anticipation of their emergence that a direct approach to the simulation of magnetization dynamics can be seriously considered.

Another issue that must be addressed with regard to demagnetizing field calculations is the extent of validity of our discrete approximation to what is basically a continuum problem. Based on simple physical arguments one expects the approximation to be reasonably accurate when the lattice constant d is smaller than the spatial scale of magnetization variations and, at the same time, d is comparable to the film thickness h.[3] Although higher order approximations with various degrees of sophistication exist,[16,17] we believe that our simple model contains the essence of the demagnetizing effect and its quantitative results can be relied on when $h \simeq d$. For films thicker than the spatial scale of magnetization variations, two-dimensional simulations are inappropriate in the first place and one must resort to three-dimensional models in order to account for Bloch points, horizontal Bloch lines,[18] and other nonuniform magnetization constructs throughout the film thickness.

B. The Landau–Lifshitz–Gilbert equation

The fundamental law governing magnetization dynamics is the mechanical law relating the applied torque to the time rate of angular momentum change. At a lattice site with dipole moment $\mathbf{m}$ and effective magnetic field $\mathbf{H}^{(\mathrm{eff})}$, the torque is $\mathbf{m}\times\mathbf{H}^{(\mathrm{eff})}$ and the angular momentum is $\mathbf{m}/\gamma$ where γ is the effective gyromagnetic ratio. Thus:

$$\dot{\mathbf{m}} = \gamma \mathbf{m}\times\mathbf{H}^{(\mathrm{eff})}. \tag{11a}$$

The effective field has contributions from external, anisotropy, exchange, and demagnetizing sources. In addition, it has a phenomenological term that represents the effect of dissipative phenomena. This term is proportional to the time rate of change of $\mathbf{m}/|\mathbf{m}|$ and, for dimensional reasons, its proportionality constant is defined as α/γ where α is the dimensionless Gilbert or viscous damping parameter.[19] Therefore:

$$\mathbf{H}^{(\mathrm{eff})} = \mathbf{H}^{(\mathrm{ext})} + \mathbf{H}^{(\mathrm{ans})} + \sum_{\mathrm{nn}} \mathbf{H}^{(xhg)} + \sum_{\mathrm{sn}} H^{(\mathrm{dmag})} + \frac{\alpha\dot{\mathbf{m}}}{\gamma|\mathbf{m}|}, \tag{11b}$$

where the total exchange field is the sum of nearest-neighbor contributions and the total demagnetizing field is the sum of significant neighbor contributions. Combining Eqs. (11a) and (11b) we obtain:

$$\dot{\theta} = -\gamma H_\phi - \alpha\dot{\phi}\sin\theta, \tag{12a}$$

$$\dot{\phi}\sin\theta = \gamma H_\theta + \alpha\dot{\theta}. \tag{12b}$$

In these equations H_θ and H_ϕ represent the total contribution of external, anisotropy, exchange, and demagnetizing fields to the effective field, namely, they are the θ and ϕ components of the sum of the first four terms on the right-hand side of Eq. (11b). One can solve Eqs. (12) for $\dot{\theta}$ and $\dot{\phi}$ to obtain:

$$\dot{\theta} = -\alpha\gamma/(1+\alpha^2)H_\theta - \gamma/(1+\alpha^2)H_\phi, \tag{13a}$$

$$\dot{\phi}\sin\theta = \gamma/(1+\alpha^2)H_\theta - \alpha\gamma/(1+\alpha^2)H_\phi. \tag{13b}$$

Equations (13) form the basis of our simulation.

If in a short time interval Δt, θ changes by $\Delta\theta$ and ϕ changes by $\Delta\phi$, the net rotation $\Delta\Psi$ of the magnetization vector will be

$$\Delta\Psi = [\,(\Delta\theta)^2 + (\Delta\phi)^2\sin^2\theta\,]^{1/2} \tag{14a}$$

so that

$$\dot{\Psi} = (\dot{\theta}^2 + \dot{\phi}^2\sin^2\theta)^{1/2}. \tag{14b}$$

In order to assure the convergence of the numerical algorithm one must keep $\Delta\Psi$ small. This and other details of the algorithm are described in Sec. IV.

C. Energy considerations

The total energy of the system is the sum of contributions from external field, anisotropy, exchange, and dipole-dipole interactions, that is,

$$E_{\mathrm{tot}} = \sum_{i,j}\left(W_{\mathrm{ext}} + W_{\mathrm{ans}} + \sum_{\mathrm{nn}}\frac{1}{2}W_{xhg} + \sum_{\mathrm{sn}} W_{\mathrm{dmag}}\right) d^2h. \tag{15}$$

The outer sum is over all lattice sites (i,j). Individual terms in Eq. (15) are

$$W_{\mathrm{ext}} = -\mathbf{H}\cdot\mathbf{M}_{ij} = -|\mathbf{M}_{ij}|(H_x\sin\theta\cos\phi + H_y\sin\theta\sin\phi + H_z\cos\theta). \tag{16}$$

W_{ans} is given by Eq. (3) and W_{xhg} is given by Eq. (6b). The factor $\frac{1}{2}$ multiplying the exchange term signifies the fact that exchange energy is mutually shared by the interacting moments; the sum is over the nearest neighbors. In the last term of Eq. (15) the sum is over significant neighbors and W_{dmag} is given by

$$W_{\text{dmag}} = -\tfrac{1}{2}\mathbf{H}^{(\text{dmag})}\cdot\mathbf{M}_{ij}$$
$$= |M_{ij}||M_{i_1 j_1}|(d^2h/2l^3)$$
$$\times\{\cos\theta\cos\theta_1 + \sin\theta\sin\theta_1$$
$$\times[\cos(\phi-\phi_1) - 3\cos(\phi-\psi)\cos(\phi_1-\psi)]\}. \quad (17)$$

Again, the factor $\frac{1}{2}$ accounts for the sharing of energy between mutually interacting dipoles.

Now let us calculate the time rate of change of energy in this system. Since E_{tot} is a function of θ_{ij} and ϕ_{ij} for all ij in the lattice and since θ_{ij} and ϕ_{ij} are the only time-dependent factors in this model, we have

$$\frac{dE_{\text{tot}}}{dt} = \sum_{ij}\left(\frac{\partial E_{\text{tot}}}{\partial\theta_{ij}}\dot{\theta}_{ij} + \frac{\partial E_{\text{tot}}}{\partial\phi_{ij}}\dot{\phi}_{ij}\right). \quad (18a)$$

Using Eqs. (4), (13), and (14) in Eq. (18a), one arrives at

$$\frac{dE_{\text{tot}}}{dt} = \frac{\alpha}{\gamma}\sum_{ij}|\mathbf{M}_{ij}|(\dot{\Psi}_{ij})^2 d^2h. \quad (18b)$$

Notice in Eq. (18b) that since γ is negative the system always loses energy during an adjustment process. The dissipative phenomena whose strength is proportional to the damping coefficient α are responsible for this energy loss; as can be observed from Eq. (18b) when $\alpha\to 0$ the rate of energy loss also approaches zero.

III. DOMAIN WALL STRUCTURE AND DYNAMICS APPROXIMATE ANALYTIC SOLUTIONS

Although the focus of this paper is on computer simulations, it is instructive to analyze the LLG equation in various limits and under different approximations in order to obtain closed form solutions for comparison with simulated results. In the following subsections we first derive the static wall structure (including Bloch lines) for both straight and circular walls. We then derive expressions for wall mobility in various limiting regimes.

A. Static domain wall equations

For a static domain wall, $\dot{\theta} = \dot{\phi} = 0$ at all lattice sites. Consequently, Eqs. (13) require that $H_\theta = H_\phi = 0$. Let us ignore the effects of demagnetizing and external fields. Then at each site on the lattice we must have

$$H_\theta^{(\text{ans})} + H_\theta^{(xhg)} = 0,$$
$$H_\phi^{(\text{ans})} + H_\phi^{(xhg)} = 0.$$

Using Eqs. (5) (without random axis anisotropy) and Eqs. (7) in the above equations, and allowing d to approach zero, in the continuum limit we obtain:

$$\sin\theta\cos\phi\nabla^2(\cos\theta) - \cos\theta\nabla^2(\sin\theta\cos\phi)$$
$$+ (K_u/A_x)\sin\theta\cos\theta\cos\phi = 0, \quad (19a)$$
$$\sin\phi\nabla^2(\sin\theta\cos\phi) = \cos\phi\nabla^2(\sin\theta\sin\phi), \quad (19b)$$

where $\nabla^2 = \partial^2/\partial x^2 + \partial^2/\partial y^2$ is the Laplacian operator in the plane. Equations (19) are the basic equations of domain wall structure in two dimensions. Note that random spatial variations of M, A_x, and K_u, random axis anisotropy, demagnetizing effects, and external field effects are not included in these equations.

To calculate wall energy, we use Eqs. (3) and (6b) and find the sum of anisotropy and exchange energies for an arbitrary lattice site. In the limit of small d we obtain

$$W(x,y) = K_u\sin^2\theta - A_x[\cos\theta\nabla^2(\cos\theta)$$
$$+ \sin\theta\cos\phi\nabla^2(\sin\theta\cos\phi)$$
$$+ \sin\theta\sin\phi\nabla^2(\sin\theta\sin\phi)]. \quad (20)$$

Here $W(x,y)$ is the local energy density arising from exchange and anisotropy contributions only. We now solve Eqs. (19) for two special cases and derive the wall energy in each case using Eq. (20).

B. Structure and energy density of straight walls

In general, θ and ϕ in Eqs. (19) are functions of both x and y. However, for straight walls, it seems reasonable to assume that θ is a function of x and ϕ is a function of y only. With this assumption Eq. (19b) reduces to

$$\frac{d^2\phi(y)}{dy^2} = 0, \quad (21)$$

which has the following solution:

$$\phi(y) = \phi_0 + (y/\Lambda_0). \quad (22)$$

Replacing this solution in Eq. (19a), one arrives at

$$\frac{d^2}{dx^2}\theta(x) = \left(\frac{1}{\Lambda_0^2} + \frac{K_u}{A_x}\right)\sin\theta\cos\theta, \quad (23)$$

which is similar to the standard equation for domain wall structure in one dimension.[19] Let us define the wall thickness parameter Δ_W as

$$\Delta_W = \left[\Lambda_0^{-2} + (\sqrt{A_x/K_u})^{-2}\right]^{-1/2}. \quad (24)$$

Equation (23) can then be integrated in the following steps:

$$\frac{d}{dx}\theta(x) = \frac{1}{\Delta_W}\sin\theta(x), \quad (25)$$

$$\frac{1}{2}\left(1+\tan^2\frac{\theta}{2}\right)\frac{d}{dx}\theta = \frac{1}{\Delta_W}\tan\left(\frac{\theta}{2}\right), \quad (26)$$

$$\frac{d}{dx}\left[\ln\left(\tan\frac{\theta}{2}\right)\right] = \frac{1}{\Delta_W}, \quad (27)$$

$$\tan\frac{\theta}{2} = \exp\left(\frac{x-x_0}{\Delta_W}\right). \quad (28)$$

Equations (22) and (28) describe the structure of a straight wall in the xy plane. x_0 is an arbitrary constant that defines the position of the wall center along the x axis. Δ_W is the wall thickness parameter given by Eq. (24) and Λ_0 is the thickness parameter for the Bloch lines within the wall. If we define Bloch lines as regions through which ϕ rotates by 180°, then the length of each of these regions in the y direction will be $\pi\Lambda_0$. Finally, ϕ_0 is an arbitrary constant that defines the position of the Bloch lines along the y axis. Note that, unlike Δ_W, Λ_0 is independent of A_x and K_u and, in the

absence of demagnetizing effects, is solely determined by the initial and boundary conditions. When Λ_0 becomes infinitely large, Bloch lines disappear, $\phi(y)$ becomes a constant (ϕ_0), and Δ_W becomes equal to $\sqrt{A_x/K_u}$ which we will denote as Δ_0; this is the standard structure for straight walls without Bloch lines. For finite values of Λ_0, however, Δ_W is always less than Δ_0, i.e., the presence of Bloch lines causes the wall width to shrink.

To calculate wall energy density, we substitute for θ and ϕ in Eq. (20) from Eqs. (22) and (28). This yields:

$$W(x,y) = K_u \sin^2\theta(x) + A_x\left[\left(\frac{d}{dx}\theta(x)\right)^2 + \frac{1}{\Lambda_0^2}\sin^2\theta(x)\right]. \quad (29)$$

The local energy density is thus independent of the y coordinate. Equation (29) can be integrated with the aid of Eq. (25) to yield the following expression for domain wall energy density σ_W:

$$\sigma_W = \int_{-\infty}^{\infty} W(x,y)dx = 4\sqrt{A_xK_u + (A_x/\Lambda_0)^2}. \quad (30)$$

Again, in the limit when Bloch lines disappear $\Lambda_0 \to \infty$ and Eq. (30) reduces to the standard expression for the wall energy density. However, for finite Λ_0, the wall energy is always greater than the energy in the absence of Bloch lines.

C. Structure and energy density of circular domain walls

In cylindrical coordinates the Laplacian operator in two dimensions is written

$$\nabla^2 = \frac{1}{r}\frac{\partial}{\partial r}\left(r\frac{\partial}{\partial r}\right) + \frac{1}{r^2}\frac{\partial^2}{\partial\beta^2},$$

where r and β are radial and azimuthal coordinates, respectively. Working in cylindrical coordinates and assuming that θ is a function of r while ϕ is a function of β only, Eqs. (19) yield

$$\phi(\beta) = \phi_0 + n_0\beta, \quad (31)$$

$$\left(r^2\frac{d^2}{dr^2} + r\frac{d}{dr}\right)\theta(r) = \left[n_0^2 + \left(\frac{K_u}{A_x}\right)r^2\right]\sin\theta(r)\cos\theta(r). \quad (32)$$

Here n_0, an integer, is equal to the number of full circle revolutions of the in-plane wall magnetization. To obtain $\theta(r)$, one must solve Eq. (32) subject to the boundary conditions $\theta(0) = 0$ and $\theta(\infty) = 180°$. This poses two problems: First, the equation is a complicated nonlinear differential equation which, most probably, does not have a simple closed form solution. Second, in the absence of external field, coercivity mechanisms, and demagnetizing effects, the equation will have a unique solution corresponding to the minimum energy domain size for the given n_0. This unique solution (interesting as it may be) is of little value in our studies, since we are primarily interested in circular domains that can have arbitrary radii. Fortunately, there is a simple approximation that can solve both problems. Consider a circular domain of radius r_0 and assume that $r_0 \gg \sqrt{A_x/K_u}$. Only in the neighborhood of r_0 is the right-hand side of Eq. (32) significantly different from zero, since when r deviates from r_0 by more than a few wall widths, $\sin\theta$ becomes essentially zero. Thus, replacing r^2 by r_0^2 on the right-hand side of Eq. (32) causes only a small error. It is now possible to solve the equation with a technique similar to the one used in solving Eq. (23). After defining the parameter ν as

$$\nu = \left[n_0^2 + (r_0/\sqrt{A_x/K_u})^2\right]^{1/2}, \quad (33)$$

one can solve Eq. (32) in the following steps:

$$r\frac{d\theta(r)}{dr} = \nu\sin\theta(r), \quad (34)$$

$$\frac{d}{dr}\left[\ln\left(\tan\frac{\theta}{2}\right)\right] = \frac{\nu}{r}, \quad (35)$$

$$\tan\frac{\theta}{2} = (r/r_0)^{\nu}. \quad (36)$$

Equations (31) and (36) describe the structure of a circular wall with radius r_0 provided that $r_0 \gg \Delta_0$ where $\Delta_0 = \sqrt{A_x/K_u}$. The wall width is a function of r_0, n_0, Δ_0, and can be calculated for specific values of these parameters. However, in the limit of small n_0, one can show that Eq. (36) is approximately the same as Eq. (28) with $\Delta_W = \Delta_0$. Thus, as expected, the wall width of large circular domains with no Bloch lines is the same as the width of straight walls.

To calculate wall energy we substitute the expressions for $\theta(r)$ and $\phi(\beta)$ in Eq. (20). This yields:

$$W(r,\beta) = K_u\sin^2\theta(r) + A_x\left[\left(\frac{d}{dr}\theta(r)\right)^2 + \frac{n_0^2}{r^2}\sin^2\theta(r)\right]. \quad (37)$$

The local energy density is thus independent of β. Equation (37) can now be integrated over the entire plane using Eq. (34) to yield the following expression for the wall energy density:

$$\sigma_W = \frac{1}{2\pi r_0}\int_0^{\infty} 2\pi r W(r,\beta)dr \approx 4\nu^{-1}(K_u r_0 + n_0^2 A_x r_0^{-1}). \quad (38)$$

In the limit of $n_0 = 0$, Eq. (38) reduces to the standard formula for domain wall energy density.

D. Domain walls in the presence of demagnetizing effects

The long range nature of dipole-dipole interactions makes exact analyses of demagnetizing effects very difficult. Nevertheless, simplifications may arise for particular geometries under certain approximations. As long as one is interested in a qualitative (or perhaps even semiquantitative) understanding of the demagnetizing effects such simplifica-

tions may be justifiable. Let us consider the straight wall with Bloch lines described by Eqs. (22) and (28). We approximate this wall with a discrete model in which the wall occupies only one row in a two-dimensional square lattice. The moments in this row are in the plane of the lattice (i.e., $\theta = 90°$) but their ϕ dependence is given by Eq. (22). All the rows to one side of the wall are "up" magnetized with $\theta = 0$ and all the rows to the other side of the wall are "down" magnetized with $\theta = 180°$. Using Eqs. (10) one calculates the demagnetizing field on individual moments within the wall as follows:

$$H_\theta^{(\mathrm{dmag})} = 0, \tag{39a}$$

$$H_\phi^{(\mathrm{dmag})} = 3(h/d)|M|\left[\sum_{n=1}^{\infty} n^{-3}\cos\left(\frac{nd}{\Lambda_0}\right)\right]\sin 2\phi. \tag{39b}$$

In the absence of Bloch lines $\Lambda_0 \to \infty$ and $\phi = \phi_0$. If we further set $h \approx d$ to assure the validity of the discrete approximation to the demagnetizing field, we obtain

$$H_\phi^{(\mathrm{dmag})} \approx 3.6|M|\sin 2\phi_0. \tag{40}$$

The coefficient 3.6 in the above equation may be off by a factor of 2 or so because of the approximations, but the general form of the equation is correct. In fact, the exact field for this special case of straight wall without Bloch lines is known to be[19]

$$H_\phi^{(\mathrm{dmag})} = 2\pi|M|\sin(2\phi_0)\sin\theta. \tag{41}$$

One can see from either Eq. (40) or Eq. (41) that two equilibrium positions of the wall ($\phi_0 = 0$ and 180°) corresponding to the Neel wall structure are unstable, while the other two positions ($\phi_0 = 90°$ and 270°) corresponding to the Bloch wall structure are stable.

When Bloch lines are present the coefficient of $\sin 2\phi$ in Eq. (39b) becomes smaller with decreasing Λ_0, but unlike the previous case there is no special value of ϕ_0 that would eliminate the demagnetizing fields altogether. (A change in ϕ_0 corresponds to a simple translation of the Bloch line array along the y axis.) Thus, the magnetic system reacts as a whole and adjusts the function $\phi(y)$ until the demagnetizing effects are canceled by the exchange fields. The largest deviations from the linear $\phi(y)$ of Eq. (22) occur around $\phi = \pm 45°$ and $\phi = \pm 135°$ as the demagnetizing field is largest in these areas.

For the approximate wall structure introduced earlier in this subsection one can also calculate the demagnetizing energy from Eq. (17). The average energy associated with the wall moments is given by

$$W_{\mathrm{dmag}} = (h/d)M^2\left[\sum_{n=1}^{\infty} n^{-3}\cos\left(\frac{nd}{\Lambda_0}\right)\right](1 - 3\langle\sin^2\phi\rangle). \tag{42}$$

The spatial average of $\sin^2\phi$ over the wall is represented by $\langle\ \rangle$ in this equation. For a wall without Bloch lines $\phi = \phi_0$, $\Lambda_0 \to \infty$, and the minimum energy states correspond to $\phi_0 = 90°$ and $\phi_0 = 270°$. For a wall with Bloch lines $\langle\sin^2\phi\rangle \approx \frac{1}{2}$. Substitution into Eq. (42) gives

$$W_{\mathrm{dmag}} \approx -\frac{1}{2}(h/d)M^2\sum_{n=1}^{\infty} n^{-3}\cos\left(\frac{nd}{\Lambda_0}\right). \tag{43}$$

Note that according to Eq. (43) the energy increases as Λ_0 decreases, so that Bloch lines repel each other even more strongly in the presence of demagnetizing forces.

For circular walls represented by Eqs. (31) and (36), one can numerically compute the demagnetizing energy on a discrete lattice using Eq. (17). For the sake of comparison with σ_W of Eq. (38), we first compute the difference in the demagnetizing energy of the lattice with and without the circular domain and then normalize this difference by the wall surface area. We denote this normalized reduction in the demagnetizing energy of a uniform lattice upon the creation of a circular domain by $\sigma_W^{(\mathrm{dmag})}$ and express it as follows:

$$\sigma_W^{(\mathrm{dmag})} = \left(\frac{1}{4\pi(r_0/d)}\sum_{ij}\sum_{i_1 j_1}\frac{\cos\theta_{ij}\cos\theta_{i_1 j_1} + \sin\theta_{ij}\sin\theta_{i_1 j_1}[\cos(\phi_{ij} - \phi_{i_1 j_1}) - 3\cos(\phi_{ij} - \psi_{iji_1 j_1})\cos(\phi_{i_1 j_1} - \psi_{iji_1 j_1})] - 1}{[(i-i_1)^2 + (j-j_1)^2]^{3/2}}\right) hM^2. \tag{44}$$

The inner sum is over significant neighbors and we chose all neighbors within a circle of radius $10d$ in our numerical calculations. The outer sum is over all lattice sites. $\psi_{iji_1 j_1}$ is the angle, in cylindrical coordinates, of the line connecting site ij of the lattice to site $i_1 j_1$ (see Fig. 1). The distribution of θ is given by Eq. (36) and is dependent on r_0/d, Δ_0/d, and n_0. The distribution of ϕ is given by Eq. (31) and is dependent on n_0 and ϕ_0. Now, for symmetry reasons, the demagnetizing energy of Eq. (44) is independent of ϕ_0 except when $n_0 = 1$. For $n_0 = 1$ the energy is minimum when $\phi_0 = 90°$, i.e., when the wall everywhere around the domain is a Bloch wall. Thus, we set $\phi_0 = 90°$ in our computations. The coefficient of hM^2 in Eq. (44) is a dimensionless quantity and is a function of r_0/d, Δ_0/d, and n_0 only.

Figure 2 is a visualization of magnetization distribution for a circular domain with $r_0/d = 10$, $\Delta_0/d = 2$, and $n_0 = 4$ on a 30×30 lattice. The arrows represent the perpendicular component of magnetization while the appendage to each arrow is the in-plane component at that site. Figure 3 shows plots of $\sigma_W^{(\mathrm{dmag})}/hM^2$ vs r_0/d for several values of n_0. It has been assumed that $\Delta_0/d = 2$ for all the curves. The lower limit for r_0/d is chosen in each case to satisfy two contrains: (i) $r_0 \geqslant 5\Delta_0$ since otherwise the approximation that allowed derivation of wall structure in Eq. (36) will be unacceptable; (ii) $r_0 \geqslant 2n_0$ since otherwise rapid variations of ϕ over the length of the wall will make our discrete approximation to the continuum problem a poor one. The interpretation of the curves is straightforward. Note that at any given radius r_0,

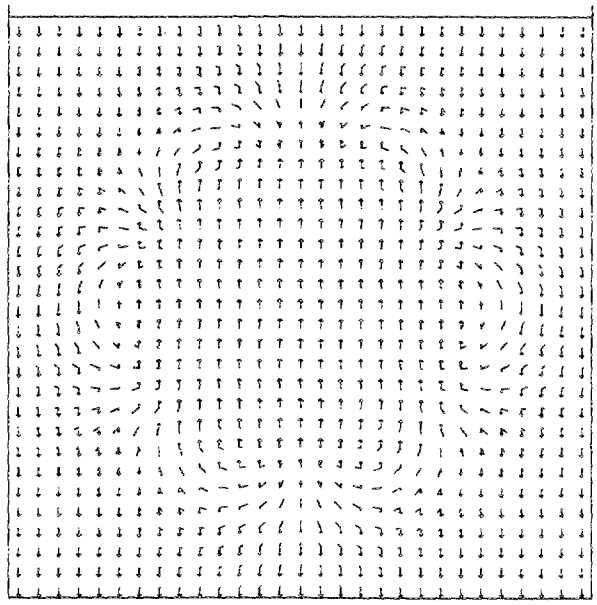

FIG. 2. Circular domain with internal wall structure. The lattice is 30×30 and the domain parameters are: $r_0/d = 10$, $\Delta_0/d = 2$, $n_0 = 4$.

the state of minimum demagnetizing energy corresponds to $n_0 = 1$. The energy increases with n_0, thus the notion that an increasing number of Bloch lines in a given wall can make up for their excess exchange energy by reducing the demagnetizing energy is false.

E. Wall motion in the presence of perpendicular dc magnetic fields

Consider the straight wall described by Eqs. (22) and (28) and assume that a perpendicular field H_z is applied. If we ignore the demagnetizing effects at this stage and postulate that the wall shape remains unchanged, then according to Eqs. (2) the only fields at work on individual moments of the lattice will be

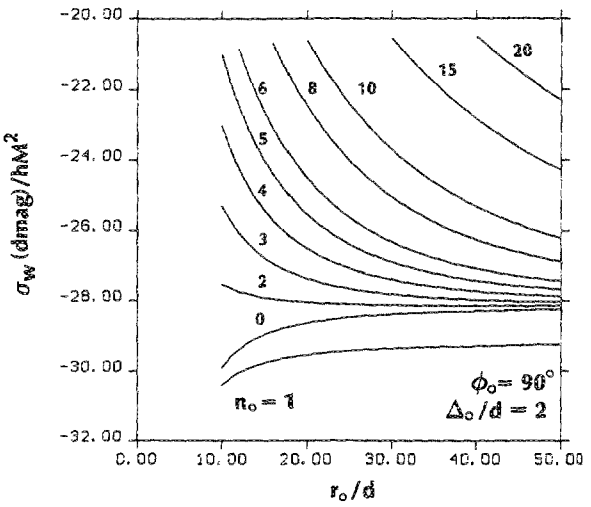

FIG. 3. Demagnetizing energy density vs domain radius for circular domains with internal wall structure. For these calculations $\Delta_0/d = 2$ and $\phi_0 = 90°$. The curve with the lowest energy corresponds to the Bloch wall structure ($n_0 = 1$).

$$H_\theta = -H_z \sin\theta, \tag{45a}$$

$$H_\phi = 0. \tag{45b}$$

Substituting in Eqs. (13) we obtain

$$\dot\theta = \frac{\alpha\gamma}{1+\alpha^2} H_z \sin\theta, \tag{46a}$$

$$\dot\phi = \frac{-\gamma}{1+\gamma^2} H_z. \tag{46b}$$

Finally, combining Eqs. (22), (25), (28), and (46), we find

$$\frac{dx_0}{dt} = -\frac{d\theta/dt}{d\theta/dx} = -\frac{\alpha\gamma\Delta_W}{1+\alpha^2} H_z, \tag{47a}$$

$$\frac{d\phi_0}{dt} = -\frac{\gamma}{1+\alpha^2} H_z. \tag{47b}$$

Obviously these uniform motions of x_0 and ϕ_0 are not cause for any change in the shape of the wall and therefore our results are consistent with earlier assumptions. From Eqs. (47) one derives expressions for wall mobility (μ_W) and Bloch line mobility (μ_L) as follows:

$$\mu_W = \frac{\alpha|\gamma|\Delta_W}{1+\alpha^2}, \tag{48a}$$

$$\mu_L = \frac{|\gamma|\Lambda_0}{1+\alpha^2}. \tag{48b}$$

As for the energy, we can substitute Eqs. (46) in Eq. (18b) to obtain (for a unit length of the wall):

$$\frac{dE_{\rm tot}}{dt} = \frac{2\alpha\gamma\Delta_W}{1+\alpha^2} MhH_z^2 = -2vhMH_z, \tag{49}$$

where $v = dx_0/dt$ is the wall velocity. The right-hand side of Eq. (49) is the expected rate of change of energy for a straight wall moving at velocity v in a medium with thickness h and magnetization M. However, we notice that part of this energy is lost to the motion of Bloch lines within the wall, without contributing to the motion of the wall itself. [Compare the terms containing $\dot\theta$ and $\dot\phi$ in Eq. (18b).] We will see later that the demagnetizing fields can block the precession of the in-plane component and thereby increase the wall mobility.

Similar arguments apply to circular domains. From Eqs. (36) and (34) one can show that

$$r_0 \frac{d\theta}{dr_0} = -r\frac{d\theta}{dr} = -v\sin\theta. \tag{50}$$

Then, using Eqs. (31), (46), and (50), one obtains

$$\frac{dr_0}{dt} = \frac{d\theta/dt}{d\theta/dr_0} = -\frac{r_0\alpha\gamma}{v(1+\alpha^2)} H_z, \tag{51a}$$

$$\frac{d\phi_0}{dt} = -\frac{\gamma}{1+\alpha^2} H_z. \tag{51b}$$

Note that for $n_0 = 0$, Eqs. (51) and (47) are identical.

Let us now look at the effects of demagnetization on wall motion. We discuss only the case of straight walls, but circular walls are qualitatively similar. The important case turns out to be the case of a wall without Bloch lines for which $\Lambda_0 \to \infty$. (The corresponding case for circular walls is $n_0 = 1$.) In the absence of the external field, the wall mini-

mizes its demagnetizing energy by settling in the Bloch wall state ($\phi = \pm 90°$). As soon as H_z is applied, the wall begins to move according to Eqs. (47). But with increasing ϕ_0 a new field, $H_\phi^{(\mathrm{dmag})}$, whose strength is given in Eq. (41), develops. Now, if H_z is small enough, a critical value of ϕ_0 is reached for which the following equality holds:

$$H_\theta = -H_z \sin\theta = \alpha H_\phi^{(\mathrm{dmag})}, \tag{52a}$$

or equivalently,

$$H_z = -2\pi\alpha|M|\sin 2\phi_0. \tag{52b}$$

When Eq. (52a) is used in Eqs. (13) we find that

$$\dot{\theta} = -(\gamma/\alpha)H_\theta, \tag{53a}$$

$$\dot{\phi} = 0. \tag{53b}$$

As before, Eq. (53a) can now be used to derive wall velocity. One obtains:

$$\frac{dx_0}{dt} = -\frac{\gamma\Delta_W}{\alpha}H_z, \tag{54a}$$

$$\phi = \phi_0, \tag{54b}$$

where ϕ_0 is given by Eq. (52b).

The wall mobility formula obtained from Eq. (54a) is the classical result first derived by Landau and Lifshitz.[20] It represents an upper bound on mobility since all the energy provided by the external field is consumed by the motion of θ while ϕ is constant [see Eq. (18b) and the discussion following Eq. (49)]. On the other hand, the mobility formula of Eq. (48a) is a lower bound since in deriving it, we placed no constraints on the motion of ϕ.[19]

F. Döring mass and Walker breakdown

Consider a straight wall without Bloch lines in the presence of demagnetizing fields and a constant perpendicular field H_z. For this wall H_θ and H_ϕ are given by Eqs. (45a) and (41), respectively (ignoring the demagnetization contribution to H_θ). Replacing in Eqs. (13) one obtains

$$\dot{\theta} = \frac{\gamma}{1+\alpha^2}(\alpha H_z - 2\pi|\mathbf{M}|\sin 2\phi)\sin\theta, \tag{55a}$$

$$\dot{\phi} = -\frac{\gamma}{1+\alpha^2}(H_z + 2\pi\alpha|\mathbf{M}|\sin 2\phi). \tag{55b}$$

From Eq. (55a) one can derive the wall velocity as was done in the preceding subsection. The result can then be combined with Eq. (55b) to eliminate the term containing $\sin 2\phi$. The final result is:

$$\frac{dx_0}{dt} = -\frac{\gamma\Delta_W}{1+\alpha^2}(\alpha H_z - 2\pi|M|\sin 2\phi), \tag{56a}$$

$$\dot{\phi} = -\gamma H_z - (\alpha/\Delta_W)\frac{dx_0}{dt}. \tag{56b}$$

Next we differentiate Eq. (56a) with respect to time, replace for $\dot{\phi}$ from Eq. (56b), and rearrange terms to obtain

$$-\left(\frac{1+\alpha^2}{2\pi\gamma^2\Delta_W\cos 2\phi}\right)\frac{d^2x_0}{dt^2} + \left(\frac{2\alpha|\mathbf{M}|}{|\gamma|\Delta_W}\right)\frac{dx_0}{dt} = 2|\mathbf{M}|H_z. \tag{57}$$

The right-hand side of this equation is the force per unit area of the wall. Therefore, the coefficient of wall acceleration must be associated with mass. For small H_z, deviation of ϕ from equilibrium ($\phi_0 = \pm 90°$) is small and therefore $\cos 2\phi \approx -1$. Also since we are concerned with walls without Bloch lines $\Delta_W = \Delta_0$. The mass per unit area of the wall, obtained from Eq. (57) under these assumptions, is known as the Döring mass and is given by

$$m_D = (1+\alpha^2)/(2\pi\gamma^2\Delta_0). \tag{58}$$

Also for a step change in H_z the time constant for the approach of velocity to equilibrium is obtained from Eq. (57) as

$$\tau = (1+\alpha^2)/(4\pi\alpha|\gamma||\mathbf{M}|). \tag{59}$$

It is clear from Eq. (52b) that there is an upper limit on H_z if Eqs. (54) are to remain valid. The maximum value of H_z is reached when ϕ_0 becomes equal to $\pm 45°$ or $\pm 135°$. This is the critical H_z for the so-called "Walker breakdown." Beyond this critical field, the initial precessional motion of the in-plane wall component does not come to a halt and the wall attains an average velocity that is somewhere between the aforementioned upper and lower bounds. When the external field is no longer small to justify the approximations that led to Eq. (54), one must first solve Eq. (55b) to obtain the function $\phi(t)$. One then uses $\phi(t)$ in Eq. (56a) and finds the time dependence of the velocity.

IV. THE SIMULATION ALGORITHM AND NUMERICAL RESULTS

There are at least two reasons for resorting to computer simulations when dealing with complex physical systems. The first reason is that in the absence of reliable analytical methods, one can postulate the underlying mechanisms of the phenomena and, through computer simulations, relate them to the observable macroscopic behavior. By comparing the simulation results with experiment, one can then verify the validity of one's assumptions and/or establish the relative significance of each postulated mechanism when several such mechanisms are simultaneously at work. The second reason is that computer simulations often provide guidance and testing ground for theoretical analysis. Their role in this respect is better appreciated when one considers the fact that theoretical studies are almost always based on simplifying approximations and their results are in many cases only indirectly related to experimental observations. The drawback is that meaningful simulations usually require an inordinate amount of computation which is beyond the reach of even the most powerful modern computers.

The advent of parallel computers with hypercube architecture in recent years has had significant implications for the study of physical systems with near-neighbor interactions. In the Connection Machine, for example, where every pair of 65 536 processors can communicate with each other in a fast and efficient manner, one has the ideal environment for the simulations of the type that is being proposed here. Since these machines are not widely available at the present time we restrict attention in this paper to the results of some small scale simulations. Besides proving the feasibility of the

algorithm, our results also shed light on certain aspects of the media for erasable optical recording.

A. The simulation algorithm

Consider an $N \times N$ square lattice where each lattice cell has dimensions $d \times d \times h$ with d being the cell size and h the film thickness. Each cell has assigned to it magnetization M, anisotropy energy density K_u, anisotropy axis (θ_0,ϕ_0), exchange stiffness coefficients A_{x1}, A_{x2}, and applied field (H_x, H_y, H_z). The two exchange coefficients represent the interaction energy with the cell to the right and the cell below, respectively. Any arbitrary distribution of magnetic parameters across the lattice is permissible although, in our preliminary simulations, we fixed all but the direction of the anisotropy axes. θ_0 and ϕ_0 in these simulations were chosen as follows:

$$\theta_0 = \pi\delta_\theta x, \tag{60a}$$

$$\phi_0 = 2\pi x. \tag{60b}$$

Here x is a uniformly distributed random variable in the interval $[0,1]$, chosen independently for each parameter and for each lattice cell. δ_θ is a constant parameter of the simulations that identifies the range of variation of θ_0. When δ_θ equals zero, the lattice has no random axis anisotropy.

It should be emphasized that the above choice of parameters is purely for simplicity's sake and that there are no experimental data for or against these assumptions at the present time. However, it is reasonable that in the absence of evidence to the contrary this simplest of models be fully scrutinized. The simulation algorithm itself is in no way dependent on the specific distribution functions, nor does the presence or absence of correlation among the various parameters alter the algorithm.

The simulation begins with an initial distribution of magnetization directions over the lattice. Next H_θ and H_ϕ are calculated for each cell using Eqs. (2), (5), (7), and (10). These values are inserted in Eqs. (13) and values of $\dot{\Psi}$ are obtained from Eq. (14b) which in turn yield a value for Δt by constraining $\Delta\Psi \simeq \dot{\Psi}\Delta t$ to be less than or equal to a certain (small) value everywhere on the lattice. Each dipole moment is then rotated by $\Delta\theta$ and $\Delta\phi$ derived from Eqs. (13) for the calculated Δt using the fourth-order Runge–Kutta technique.[21] The lattice thus arrives at a new state where each moment has a new orientation. The energy of this state is calculated from Eqs. (3), (6b), (16), and (17) and the process is repeated.

The pattern of magnetization will be displayed using the following convention: each moment is represented by its projections on the plane of the lattice ($\parallel$ component) and perpendicular to the lattice ($\perp$ component). The perpendicular component will have an arrowhead pointing either up or down depending on whether the moment is above or below the plane of the lattice. The size of the arrowhead will be proportional to the magnitude of the $\perp$ component itself, so in case of ambiguity one should be guided by this bit of information. To give an example, $\uparrow$—— is a moment above the plane with the perpendicular component equal to the arrow, and the in-plane component along the appendage to the arrow, pointing towards the upper right-hand corner of the plane. The origin is the point where the two components join each other and as such the direction of the in-plane component is uniquely identifiable without the need for another arrowhead. Another example is ——$\downarrow$ which has a small perpendicular component, is below the plane of the lattice, and points to the left.

B. Results and discussion

Preliminary simulations of a 30×30 square lattice were run on a VAX 11/780 machine in order to study the performance of the algorithm. The following set of parameters was used throughout: $M = 100$ emu/cm^3, $K_u = 10^6$ erg/cm^3, $A_x = 10^{-7}$ erg/cm, $d = 10$ Å, $\gamma = -10^7$ Oe^{-1} s^{-1}, and $\alpha = 0.5$. The maximum rotation across the lattice $(\Delta\Psi)_{\max}$ for each iteration was set at 2° and the scanning of the lattice was performed in a straightforward sequential way. Since the long-range nature of demagnetizing fields results in a substantial increase of computation time, these fields were not included in our simulations. However, there is no fundamental reason for this exclusion and, with highly parallel computers, it should be possible to retain the demagnetizing effects even in large scale simulations.

According to the standard theory of domain walls the preceding set of parameters corresponds to the following values of wall thickness and energy density:

$$\pi\Delta_0 = \pi\sqrt{A_x/K_u} = 99.4 \text{ Å}, \tag{61a}$$

$$\sigma_W = 4\sqrt{A_x K_u} = 1.26 \text{ erg/cm}^2. \tag{61b}$$

Also, contributions of exchange and anisotropy to the wall energy must be equal. In the absence of demagnetizing effects the wall mobility is given by Eq. (48a) as

$$\mu_W = \alpha|\gamma|\Delta_0/(1+\alpha^2) = 12.65\times10^{-3} \text{ m/s/Oe}, \tag{61c}$$

where straight wall motion is accompanied by the precessional motion of the in-plane wall magnetization. These theoretical predictions can now be compared with numerical results.

Consider the situation where random axis anisotropy is absent, namely $\delta_\theta = 0$. Initially ten columns on the left of the lattice are made to point up while the remaining twenty columns point down. The lattice elements in the leftmost column and those in the rightmost column remain frozen in their initial orientations while periodic boundary conditions apply to the top and bottom rows. Figure 4(a) shows the state of the lattice after 1000 iterations. Clearly the abrupt transition has relaxed into a wall of approximately 100 Å thickness while the in-plane components of magnetization are parallel throughout the wall. Figure 4(b) shows the exchange energy, the anisotropy energy, and the total energy of the system versus time. It is observed that for the first ten or so picoseconds the system slowly moves away from its initial configuration which is an unstable, maximum energy state. After this period the torques become strong enough to pull the lattice down to its minimum energy state. Then, after a few oscillations, the wall assumes its steady configuration and all the energy terms reach a stable value. Note that the final value of the exchange energy is only slightly above the anisotropy energy. The total energy, when divided by the

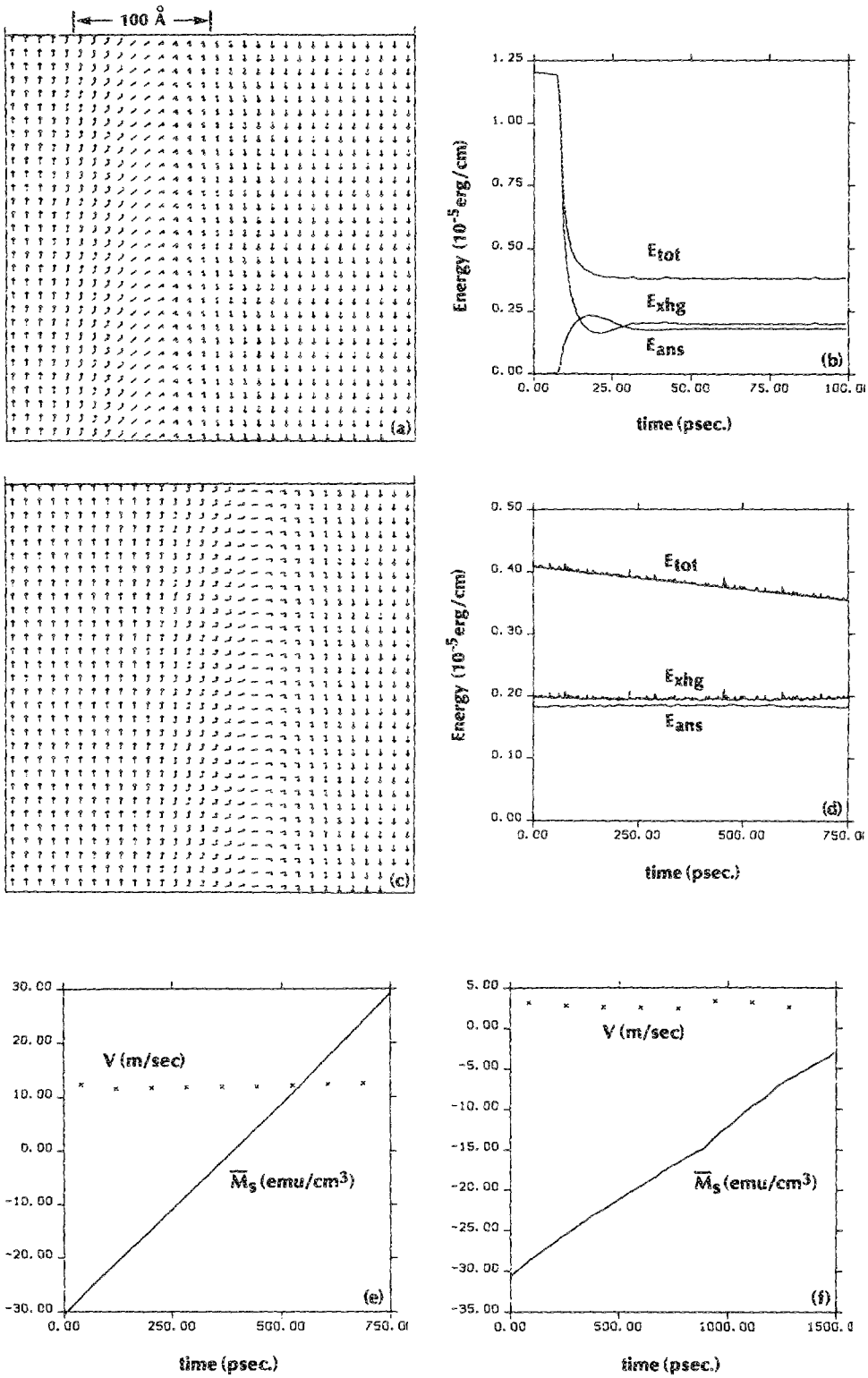

FIG. 4. Domain wall structure and dynamics for a medium with $M_s = 100$ emu/cm^3, $K_u = 10^6$ ergs/cm^3, $A_x = 10^{-7}$ ergs/cm, $d = 10$ Å, $\gamma = -10^7$ Oe^{-1} s^{-1}, and $\alpha = 0.5$. It is assumed that the medium has perfect uniaxial anisotropy in the perpendicular direction, i.e., $\delta_\theta = 0$. (a) Straight wall created from an initial condition with ten columns on the left pointing up and the remaining twenty columns pointing down. The pattern is obtained after 1000 iterations, corresponding to $t = 163$ ps. (b) Exchange energy, anisotropy energy, and total energy of the magnetic system during the relaxation process that starts with the unstable initial configuration and ends with the stable wall structure in (a). (c) Under an applied field $H_{ext} = 1$ kOe the wall in (a) moves to the right. The pattern is obtained after 4000 iterations corresponding to $t = 658$ ps. (d) Exchange energy, anisotropy energy, and total energy of the magnetic system under the applied field $H_{ext} = 1$ kOe. While the wall energy consisting of exchange and anisotropy contributions remains constant, the external field energy decreases linearly with time. (e) Average lattice magnetization vs time under the applied field $H_{ext} = 1$ kOe. The initial state of the lattice is shown in (a). The linear increase of the average magnetization with time corresponds to a constant wall velocity of 12.8 m/s, obtained from the average slope of the curve during several time intervals as indicated by the symbols $\times$. (f) Same as (e) except that $H_{ext} = 250$ Oe. The average wall velocity is 2.8 m/s.

length of the wall (300 Å), gives a value of $\sigma_w = 1.3$ ergs/cm^2, in good agreement with Eq. (61b).

Although the energy reaches a stable value after only a few hundred iterations, the average magnetization of the lattice requires a few thousand iterations to become stable. However, no significant changes in the structure of the wall were observed during this stabilization process. We noticed that stabilization was somewhat dependent on the details of the numerical integration procedure and on the way in which the lattice is scanned. For instance, if $(\Delta\Psi)_{max}$ is made larger or if the lattice is scanned in a checkerboard fashion, the stability of average magnetization is achieved in a shorter period of time.

When a perpendicular field $H_{ext} = 1$ kOe is applied to the lattice of Fig. 4(a), the wall embarks on a translational motion during which the wall structure remains intact but its in-plane component gyrates around the field. Figure 4(c) shows the lattice after 4000 iterations under the applied field. The various energies of the system during the period of wall translation are shown in Fig. 4(d). Notice that the exchange and anisotropy energies remain more or less constant but the external field energy drops linearly with time. Figure 4(e) shows the average magnetization versus time of motion. The wall velocity of 12.8 m/s obtained from this curve is in excellent agreement with the theoretical value of Eq. (61c).

If the applied field to the lattice of Fig. 4(a) is $H_{ext} = 250$ Oe instead, the wall velocity will reduce to 2.8 m/s as shown in Fig. 4(f). Although this velocity is not quite the same as the theoretical value of $v = 3.16$ m/s, the error is only about 10%. The reason for the reduced accuracy is probably the increased significance of numerical errors in relation to the external field. In any event, this example shows that simulation results are in fact reliable and could yield reasonable estimates of the various performance characteristics of the media.

Next we consider the effect of random axis anisotropy on the structure and dynamics of straight walls. The parameters will be the same as before except for δ_θ which is now 0.25. This means that anisotropy axes will have random orientations (θ_0,ϕ_0) with θ_0 chosen from a uniform distribution in the interval $(0,\pi/4)$ and ϕ_0 chosen independently from another uniform distribution over $(0,2\pi)$. The wall structure in this case depends on the seed for the random number generator or, what amounts to the same thing, the initial position of the wall in the lattice. We studied two cases with identical seeds but different initial distributions. In the first case the abrupt transition from up to down magnetization was placed at column 20 of the lattice and subsequent behavior of the system was as depicted in Fig. 5. The second case had the abrupt transition placed at column 10 which resulted in the patterns of Fig. 6. The wall structure in Fig. 5(a) has a 2π-Bloch line and is stabilized after 17 000 iterations although the energy of the lattice, shown in Fig. 5(b), reaches the steady state after only a few hundred iterations. Notice in Fig. 5(b) that, unlike the previous case, the anisotropy energy of the initial state is nonzero. This, of course, is due to the presence of random axis anisotropy. Once the wall is established, the exchange and anisotropy energies of the system become almost equal and the wall energy density approaches 1.94 ergs/cm^2. There is no meaningful comparison between this and the wall energy density obtained in the previous case, since in the present situation the energy is not confined to the wall region but has contributions from the rest of the lattice as well. The equality of exchange and anisotropy energies must also be considered coincidental.

Figure 5(c) shows the state of the lattice after 3000 iterations in the presence of an applied perpendicular field $H_{ext} = -1$ kOe; the energy versus time curves of Fig. 5(d) confirm that the wall structure during motion has remained intact. The behavior of average magnetization during wall motion as depicted in Fig. 5(e) shows a slight nonuniformity in velocity which is expected since the wall has to traverse a region with random distribution of anisotropy axes. The average wall velocity in the 500-ps time interval elapsed between Figs. 5(a) and 5(c) is 19.7 m/s which is significantly higher than the 12.8-m/s velocity in Fig. 4(e). This difference can be attributed to the gyration of the in-plane component of wall magnetization: Whereas the wall of Fig. 4 can freely gyrate in the plane of the lattice and thereby cause a reduction of the translational velocity, the in-plane component in Fig. 5 is constrained by the local orientations of the axes of anisotropy and its gyration is reduced, causing an increase in the translational velocity. Of course, the addition of demagnetizing fields with the constraints that they impose on the in-plane gyration will further change the picture, as can be expected from the theoretical considerations in Sec. III.

Finally, Fig. 5(f) shows the average magnetization versus time when the wall of Fig. 5(a) is subjected to an external field $H_{ext} = -250$ Oe. The wall initially moves to the left, but then it encounters an insurmountable barrier, retreats to the right, and comes to rest near its initial location. One can associate this behavior with wall coercivity.

Figure 6 is obtained under conditions identical to those of Fig. 5 except for the initial wall position. Note that here the wall has no internal structure and, as a result, its energy density is 1.6 ergs/cm^2 which is well below the energy of the wall in Fig. 5. The wall velocity under an applied field $H_{ext} = 1$ kOe is again nonuniform with an average of 15.4 m/s, which is between those obtained for Figs. 4 and 5, indicating that the in-plane gyration has increased in comparison with the wall with internal (Bloch line) structure but is still less than it would be in the absence of random axis anisotropy. When the applied field is $H_{ext} = 250$ Oe, the average velocity drops to $v = 5.2$ m/s. Notice that between Figs. 6(e) and 6(f) the field has dropped by a factor of 4 but the velocity has only dropped by a factor of 3. The reason for this departure from linearity may be that barriers to the in-plane gyration that could be overcome with the larger field have now become effective in slowing down the gyration under the smaller field, thereby causing the translational velocity to increase. Comparing the results of this example with those of the previous one, one might also conclude that wall coercivity depends not only on the material characteristics but also on the structure of the wall itself.

To study the effect of spatial variations of magnetic parameters, the small circular region at the center of the lattice in Fig. 7 was assigned a value of $K_u = 10^7$ erg/cm^3. All other

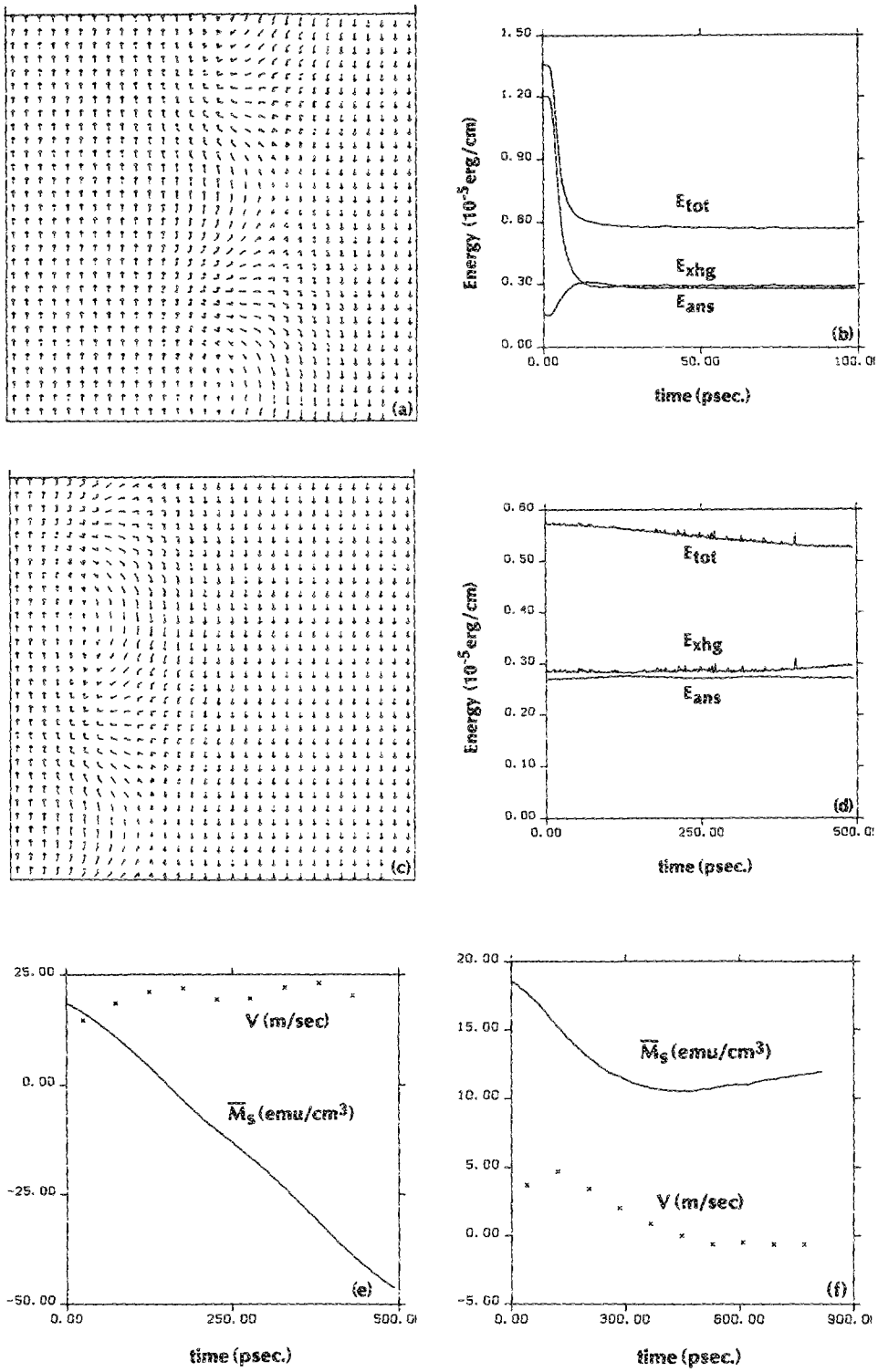

FIG. 5. Domain wall structure and dynamics for a medium with $M_s = 100$ emu/cm^3, $K_u = 10^6$ ergs/cm^3, $A_x = 10^{-7}$ ergs/cm, $d = 10$ Å, $\gamma = -10^7$ Oe^{-1} s^{-1}, and $\alpha = 0.5$. It is assumed that the medium has random axis anisotropy with $\delta_\theta = 0.25$. (a) Straight wall created from an initial condition with twenty columns on the left pointing up and the remaining ten columns pointing down. The pattern is obtained after 17 000 iterations, corresponding to $t = 2740$ ps. (b) Exchange energy, anisotropy energy, and total energy of the magnetic system during the relaxation process that starts with the unstable initial configuration and ends with the stable wall structure in (a). (c) Under an applied field $H_{ext} = -1$ kOe the wall in (a) moves to the left. The pattern is obtained after 3000 iterations corresponding to $t = 495$ ps. (d) Exchange energy, anisotropy energy, and total energy of the magnetic system under the applied field $H_{ext} = -1$ kOe. While the wall energy consisting of exchange and anisotropy contributions remains relatively constant, the external field energy decreases with time. (e) Average lattice magnetization vs time under the applied field $H_{ext} = -1$ kOe. The initial state of the lattice is shown in (a). The decreasing magnetization vs time curve represents a variable wall velocity as indicated by the symbols $\times$. The average velocity is about 19.7 m/s. (f) Same as (e) except that $H_{ext} = 250$ Oe. The applied field is not large enough to overcome the barriers to wall motion created by the random axis anisotropy.

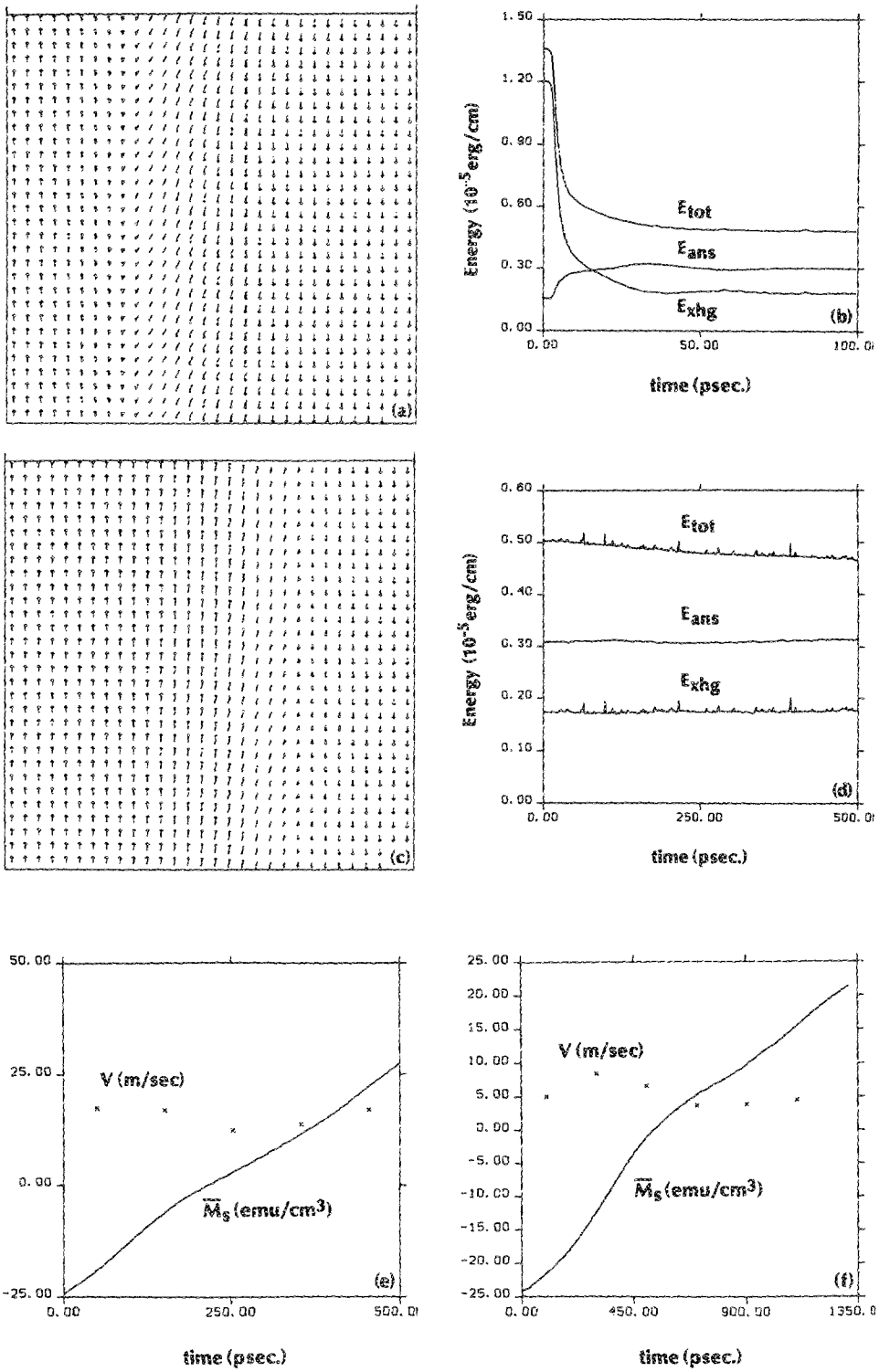

FIG. 6. Domain wall structure and dynamics for a medium with $M_s = 100$ emu/cm^3, $K_u = 10^6$ ergs/cm^3, $A_x = 10^{-7}$ ergs/cm, $d = 10$ Å, $\gamma = -10^7$ Oe^{-1} s^{-1}, and $\alpha = 0.5$ It is assumed that the medium has random axis anisotropy with $\delta_\theta = 0.25$. (a) Straight wall created from an initial condition with ten columns on the left pointing up and the remaining twenty columns pointing down. The pattern is obtained after 19 000 iterations, corresponding to $t = 3043$ ps. (b) Exchange energy, anisotropy energy, and total energy of the magnetic system during the relaxation process that starts with the unstable initial configuration and ends with the stable wall structure in (a). (c) Under an applied field $H_{ext} = 1$ kOe the wall in (a) moves to the right. The pattern is obtained after 3000 iterations corresponding to $t = 489$ ps. (d) Exchange energy, anisotropy energy, and total energy of the magnetic system under the applied field $H_{ext} = 1$ kOe. While the wall energy consisting of exchange and anisotropy contributions remains constant, the external field energy decreases with time. (e) Average lattice magnetization vs time under the applied field $H_{ext} = 1$ kOe. The initial state of the lattice is shown in (a). The increase of magnetization with time corresponds to a variable wall velocity as indicated by the symbols $\times$. The average velocity is about 15.4 m/s. (f) Same as (e) except that $H_{ext} = 250$ Oe. The average wall velocity is 5.2 m/s.

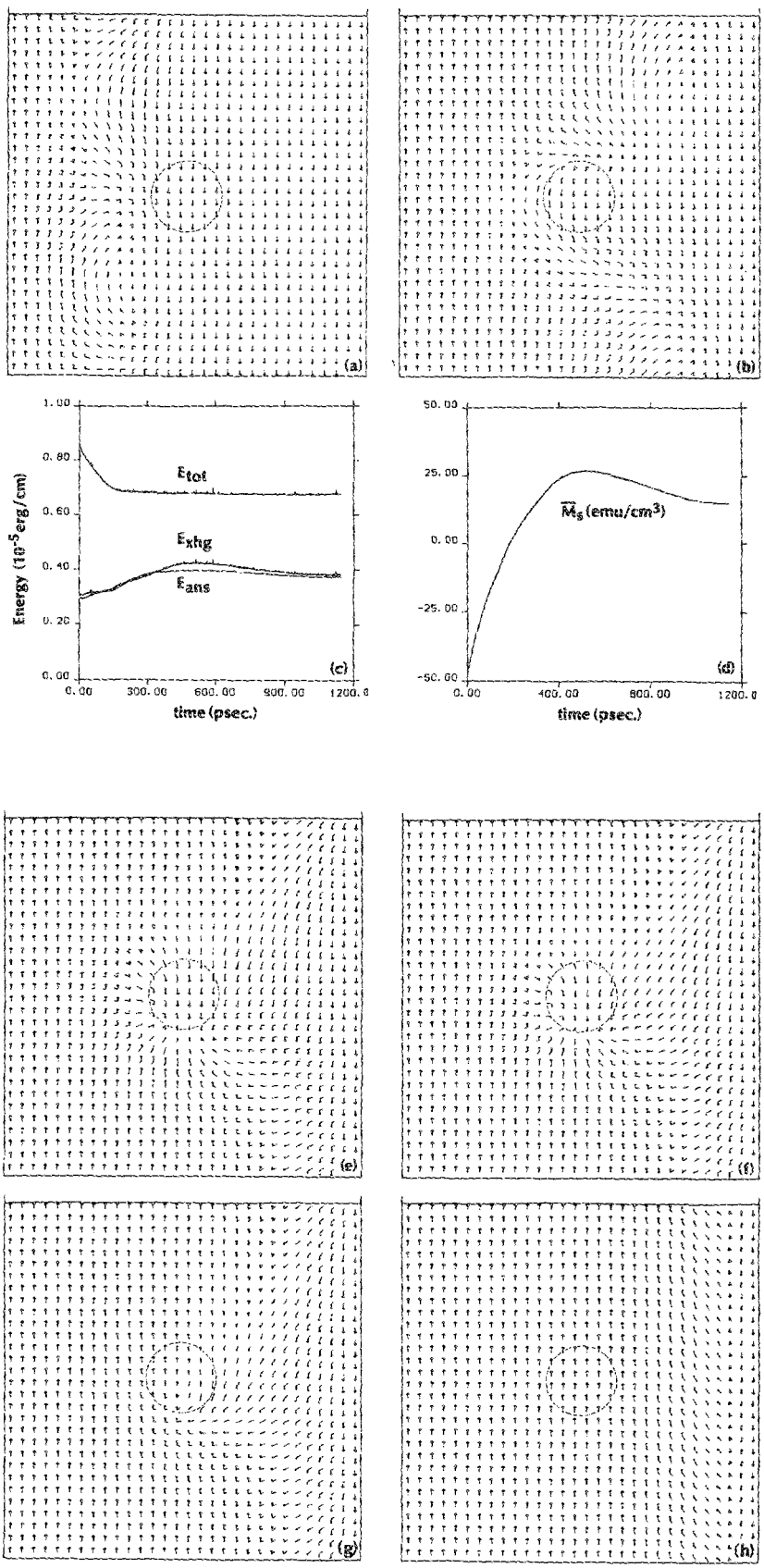

FIG. 7. Domain wall structure and dynamics for a medium with $M_s = 100$ emu/cm^3, $K_u = 10^6$ ergs/cm^3, $A_x = 10^{-7}$ ergs/cm, $d = 10$ Å, $\gamma = -10^7$ Oe^{-1} s^{-1}, and $\alpha = 0.5$. It is assumed that the medium has random axis anisotropy with $\delta_\theta = 0.25$. Also in the central region $K_u = 10^7$ ergs/cm^3. (a) Straight wall created from an initial condition with ten columns on the left pointing up and the remaining twenty columns pointing down. The pattern is obtained after 5000 iterations, corresponding to $t = 731$ ps. (b) Under an applied field $H_{ext} = 6$ kOe the wall bends around the central high anisotropy region. The pattern is obtained after 8000 iterations corresponding to $t = 1145$ ps. (c) Exchange energy, anisotropy energy, and total energy of the magnetic system under the applied field $H_{ext} = 6$ kOe. While at times the wall energy consisting of exchange and anisotropy contributions increases, the total energy always decreases. (d) Average lattice magnetization vs time under the applied field $H_{ext} = 6$ kOe. The initial state of the lattice is shown in (a). Under an applied field $H_{ext} = 7$ kOe the wall in (a) moves past the central barrier. The patterns in (e), (f), (g), and (h) correspond to $t = 326$ ps, 438 ps, 457 ps, and 600 ps, respectively. (i) Exchange energy, anisotropy energy, and total energy of the magnetic system under the applied field $H_{ext} = 7$ kOe. The sharp drop around $t = 450$ ps represents the disappearance of the central domain. (j) Average lattice magnetization vs time under the applied field $H_{ext} = 7$ kOe. The initial state of the lattice is shown in (a).

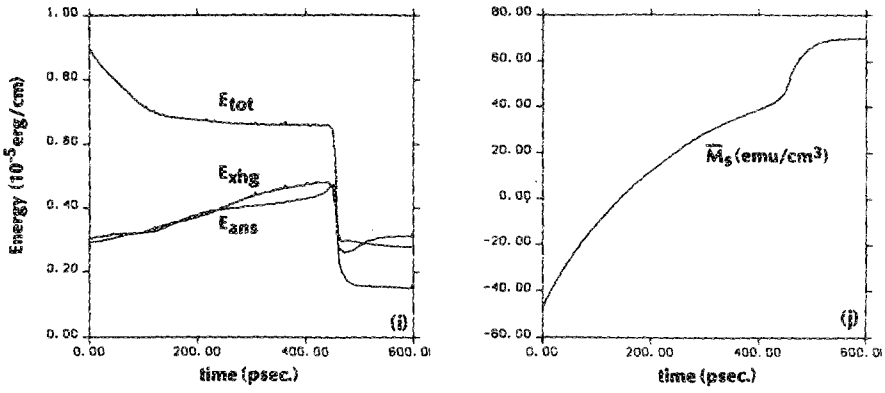

FIG. 7 (*continued*).

parameters were the same as Fig. 6. An abrupt transition placed at column 10 relaxes into the wall (with a 2π-Bloch line) shown in Fig. 7(a). Application of the external field $H_{ext} = 6$ kOe results in a bent wall around the central region shown in Fig. 7(b). While the exchange and anisotropy energies of the system increase in the process of bending, the total energy decreases due to the reduction in the external field energy [see Fig. 7(c)]. The average magnetization versus time for this process is shown in Fig. 7(d). Under an external field $H_{ext} = 7$ kOe the barrier was overcome and the wall moved all the way to the right. The sequence of events in this case is shown in Figs. 7(e)–7(h). The interesting feature of these figures is that they show the wall not going through the barrier but around it, and that the central region is reversed in the wake of the wall. Figure 7(i) shows the energies of the lattice under the external field $H_{ext} = 7$ kOe. The sharp drop around $t = 450$ ps signals the reversal of the central region. Figure 7(j) is the plot of average magnetization versus time and shows the corresponding sharp rise at the time of annihilation of the central domain.

V. CONCLUDING REMARKS

A discrete model for the computer simulation of magnetization dynamics in thin films of amorphous magnetic materials has been presented. The model incorporates the effects of exchange, anisotropy, external field and demagnetization, with provisions to include spatial variations of the various magnetic parameters. The Landau–Lifshitz–Gilbert equation is the basis of this work. For certain ideal situations where analytic solutions to the LLG equation exist we have provided detailed analyses, with results that provide useful benchmarks for testing the simulation algorithm. Preliminary results of small scale simulations on a VAX 11/780 machine confirmed the robustness of the algorithm and, in special cases where analytic solutions exist, excellent agreement with theory was demonstrated. As an example of applications in the study of complex phenomena, the effects of random axis anisotropy on the structure and dynamics of stright walls were also investigated. The simulation software for the Thinking Machines Corporation's Connection Machine is currently under development and we hope to present more elaborate results of this work in the near future.

ACKNOWLEDGMENTS

I wish to express my gratitude to Professor R. Brower, Professor R. Giles, and Professor M. Ruane of Boston University and Dr. T. W. McDaniel of the IBM Corporation for many helpful discussions. This project is supported by a grant from the IBM Corporation.

[1]H.-P. D. Shieh and M. H. Kryder, J. Appl. Phys. **61**, 1108 (1987).
[2]H.-P. D. Shieh and M. H. Kryder, Appl. Phys. Lett. **49**, 473 (1986).
[3]M. Mansuripur, J. Appl. Phys. **61**, 1580 (1987).
[4]J. C. Suits, R. H. Geiss, C. J. Lin, D. Rugar, and A. E. Bell, Appl. Phys. Lett. **49**, 419 (1986).
[5]M. Mansuripur, J. Appl. Phys. **61**, 3334 (1987).
[6]S. Matsushita, K. Sunago, and Y. Sakurai, IEEE Trans. Magn. **11**, 1109 (1975).
[7]M. Urner-Wille, R. Kobs, and K. Witter, IEEE Trans. Magn. **17**, 2621 (1981).
[8]S. Honda, J. Hirokane, M. Ohkoshi, and T. Kusuda, J. Magn. Magn. Mater. **35**, 208 (1983).
[9]Y. Mimura, N. Imamura, and T. Kobayashi, Jpn. J. Appl. Phys. **15**, 933 (1976).
[10]W. D. Hillis and G. Steele, Comm. ACM **29**, 1170 (1986).
[11]W. D. Hillis, Sci. Am. **256**, 108 (June 1987).
[12]J. C. Mallinson, IEEE Trans. Magn. **23**, 2003 (1987).
[13]M. Mansuripur and M. F. Ruane, IEEE Trans. Magn. **22**, 33 (1986).
[14]A. Gangulee and R. C. Taylor, J. Appl. Phys. **49**, 1762 (1978).
[15]J. D. Jackson, *Classical Electrodynamics* (Wiley, New York, 1975).
[16]C. C. Shir, J. Appl. Phys. **49**, 3413 (1978).
[17]M. E. Schabes and A. Aharoni, IEEE Trans. Magn. **23**, 3882 (1987).
[18]B. E. MacNeal and F. B. Humphrey, IEEE Trans. Magn. **15**, 1272 (1979).
[19]A. P. Malozemoff and J. C. Slonczewski, *Magnetic Domain Walls in Bubble Materials* (Academic, New York, 1979).
[20]L. Landau and E. Lifshitz, Phys. A. Soviet Union **8**, 153 (1935).
[21]F. B. Hildebrand, *Introduction to Numerical Analysis* (McGraw-Hill, New York, 1956).